Synthesis and magnetic behavior of ultra-small bimetallic FeCo/graphite nanoparticles

M Castrillón[1], A Mayoral[2], A Urtizberea[3], C Marquina[3,4], S Irusta[5,6], J G Meier[1] and J Santamaría[5,6]

[1] Technological Institute of Aragon (ITA), Maria de Luna 8, E-50018, Zaragoza, Spain [2] Advanced Microscopy Laboratory (LMA), Nanoscience Institute of Aragon (INA), Universidad de Zaragoza, Mariano Esquillor s/n, E-50018, Zaragoza, Spain
[3] Instituto de Ciencia de Materiales de Aragón (ICMA), CSIC-Universidad de Zaragoza, Pedro Cerbuna 12, Zaragoza, E-50009, Spain
[4] Departamento de F´ısica de la Materia Condensada, Universidad de Zaragoza, Pedro Cerbuna 12, Zaragoza, E-50009, Spain
[5] Department of Chemical Engineering, Nanoscience Institute of Aragon (INA), University of Zaragoza, E-50018 Zaragoza, Spain
[6] Networking Research Center on Bioengineering, Biomaterials and Nanomedicine, CIBER-BBN, Spain

E-mail: sirusta@unizar.es

Abstract

FeCo-alloy graphite-coated nanoparticles with mean particle diameter under 8 nm have been synthesized following a CVD carbon-deficient method. The superior magnetic properties of FeCo-alloy nanoparticles makes them good candidates to be used as magnetic filler in magneto-polymer composites. Thanks to the protective effect of the graphite shell, FeCo nanoparticles are stable under oxygen atmosphere up to 200 °C. The as-prepared nanoparticles presented a highly long range chemically ordered core being ferromagnetic at room temperature with a saturation magnetization at room temperature close to the bulk value. After annealing at 750 K the saturation magnetization and the coercive field increase. To investigate the processes involved in the thermal treatment, the temperature dependence of the magnetization and the particle composition, size and structure have been characterized before and after annealing. Besides powder x-ray diffraction (XRD) and x-ray photoelectron spectroscopy (XPS), a detailed study by means of advanced transmission electron microscopy (TEM) techniques has been carried out. In particular, aberration corrected scanning transmission electron microscopy (STEM), has shown that nanoparticles became faceted after the thermal treatment, as a mechanism to reach the thermodynamic equilibrium within the metastable phase. This outstanding feature, not previously reported, leads to an increase of the shape anisotropy, which in turn might be the origin of the observed increase of the coercive field after annealing.

1. Introduction

Stimuli-responsive materials have attracted scientists' interest over the lasts years due to their biomimetic behavior and their potential use in intelligent devices. Smart polymers are increasingly playing an important role in a wide range of applications, especially in the biomedical, coatings and microelectronics fields [50]. Contrary to intelligent devices limited by diffusion processes (of either heat or mass), those directly operated by exposure to a field (magnetic or electric) can have shorter response times. To prepare highly efficient magneto-responsive materials, the 'filling' of polymer materials with magnetic nanoparticles appears to be an appealing and efficient solution [33, 45].

In order to perfectly control the amplitude of the desired magnetic response, as well as to anticipate the properties of these magnetic–polymer composites, many parameters need to be controlled, especially of the nanostructure/composition of the composite: magnetic material loading, compatibility between the polymer and magnetic phases (surface coating), magnetization and the functional properties of the magnetic fillers (nanoparticles) in their working temperature range [50]. In this work we will focus on the last subject.

Alloys of Fe, Co, and Ni present outstanding magnetic properties such as very high magnetization, low coercive forces, and very low magnetostriction, required in soft magnetic materials for power applications such as transformers, inductive devices, etc. Specifically, FeCo-alloy nanoparticles have gained significant interest due to their superior magnetic properties of very high Curie temperature, low coercivity, low magnetocrystalline anisotropy, high permeability, and high saturation magnetization (M_s) [30, 49].

FeCo-alloy-based nanoparticles have been prepared by a wide variety of techniques such as thermal decomposition of bimetallic carbonyl precursors [43, 55], reductive decomposition of organometallic precursors [7], sonoelectrochemical techniques [63], polyol-assisted processes [19, 21] and chemical vapor deposition [61]. However, post-synthetic handling and processing of these nanoparticles presents significant challenges due to their poor chemical stability when exposed to atmospheric conditions. Additionally, some applications require the ability to operate at high temperatures while keeping the alloy functional properties. One of the proposed solutions involved the encapsulation of FeCo-alloy magnetic nanoparticles in a carbon-based shell to prevent their degradation in reactive chemical environments at the same time as improving compatibility with polymer matrices. The carbonaceous shell has the additional advantage of isolating the particles, separating them from each other, to decrease/avoid close-proximity magnetic interactions [24]. To this end, different carbon coating strategies have been developed [8, 15, 26, 35, 40, 44, 52, 53, 56, 57], although many of these methods suffer from various drawbacks such as being a complex procedure and the poor size and growth control of the nanoparticles. One of the best alternatives seems to be a multilayered graphitic coating by a chemical vapor deposition (CVD) [46], a method whose feasibility has been proved in related FeNi-alloy and NiCo-alloy systems [5]. This route employs a carbon-deficient atmosphere to obtain ultra-small superparamagnetic nanoparticles as individual entities, non-agglomerated and stable at room temperature.

In this work nanoparticles of $Fe_{50}Co_{50}$ alloy coated with graphite (hereinafter termed FeCo/CG nanoparticles), oriented to stimuli-responsive composite application, have been synthesized using the above-mentioned CVD technique. Although the magnetic properties of FeCo nanoparticles encapsulated in carbon/graphitic shells have been previously reported [10, 17, 18, 24, 28, 44, 46, 47, 53, 59], an extensive study of their magnetic and structural properties should be carried out in the temperature regime in which they are potentially applicable, especially when high temperatures are involved in targeted applications. In our case this is mandatory due to the procedure used subsequently for incorporating the FeCo/CG nanoparticles into the polymer composite (melt mixing method) [33, 45].

Our study of the changes observed in the FeCo/CG nanoparticles before and after heating includes a comprehensive chemical and structural characterization based on image analysis and compositional measurements at atomic scale by means of C_s corrected STEM. The results obtained are decisive for understanding how the temperature affects their functionality properties—
i.e. the correlation between the chemical composition, structure and size of FeCo nanoparticles and their magnetic behavior, within the working temperature range.

2. Experimental section

The synthesis of the carbon-coated alloy nanoparticles was carried out following the procedure given by Seo *et al* [46]. The precursors were prepared by impregnation of fumed silica (Aerosil ® 300) with methanol solution (CH_4OH) of iron nitrate $Fe(NO_3)_3 \cdot 9H_2O$ and cobalt nitrate $Co(NO_3)_2 \cdot 6H_2O$ with a Fe/Co molar ratio of 1:1 and weight $FeCo/SiO_2$ ratio of 0.043. The suspension was sonicated for 60 min, then methanol was removed by evaporation and the solid dried at 60 °C overnight. The obtained material was placed inside a quartz tube (2.5 cm diameter, 50 cm length), then placed inside an electrical oven and heated up to 800 °C, using a heating rate of 2.6 °C min^{-1} under hydrogen flow of 100 ml min^{-1} to form the FeCo alloy. The graphitic layer coating was produced by decomposition of a methane flow of 800 ml min^{-1} during 5 min. The generated nanoparticles were then fast cooled down to room temperature under nitrogen atmosphere. Finally, the silica support was removed by etching with a solution of hydrofluoric acid (HF) (reagent grade >40%).

XRD analysis was performed on a Rygaku/Max System RU 300 diffractometer, operating at a voltage of 40 kV and a current of 80 mA with graphite-monochromatized Cu Kα (λ=0.154 05 nm) radiation. Morphology, microstructure and compositional studies were performed by conventional transmission electron microscopy (TEM), bright field (BF) and high-angle annular dark field (HAADF) spherical aberration corrected (C_s) scanning transmission electron microscopy (STEM) combined with energy dispersive x-ray spectrometry (EDS) and electron energy loss spectroscopy (EELS) analysis in a FEI Tecnai F30 and in a probe aberration corrected FEI Titan 60-300, both operated at 300 kV and equipped with an EDAX x-rays microanalysis system and a Gatan Tridiem energy filter. The magnetic properties of the FeCo/CG nanoparticles were investigated by magnetization measurements in a Quantum Design MPMS with a superconducting SQUID magnetometer. Raman spectroscopy was used to characterize the carbon shell; the Raman spectrum was recorded with a TRS-600-SZ-P Jasco laser Raman instrument; the excitation source was the 514.5 nm line of a Spectra 9000 Photometrics Ar ion laser. The laser power was set at 30 mW (resolution 4 cm^{-1}).

The amount of graphite/carbon forming the nanoparticles layers was determined by means of thermal gravimetric analysis (TGA) under oxidative atmosphere at a heating rate of 5 °C min^{-1} from 30 to 900 °C in a Pyris1 TGA (Perkin-Elmer). The existence of structural and magnetic temperature induced transitions changes in the nanoparticles were assessed in the same Pyris1 TGA equipment adapted with a permanent magnet (50 Oe in sample) and a Perkin-Elmer Diamond differential scanning calorimeter (Diamond DSC), respectively; both were operated at heating rate of 5 °C min^{-1} under 20 ml min^{-1} continuous N_2 flow.

Surface composition of as-prepared samples was analyzed by x-ray photoelectron spectroscopy (XPS) using an Axis Ultra DLD (Kratos Tech.). The spectra were excited by the Mg Kα source (1253.6 eV) run at 12 kV and 10 mA. For the individual peak regions pass energy of 20 eV was used. Each survey spectrum was measured at 160 eV pass energy.

3. Results and discussion

Powder x-ray diffraction was used to study the phases formed after the FeCo/CG synthesis and silica elimination. Figure 1 shows the presence of well-defined peaks at 2θ values of 43.89° and 65.29° corresponding to the crystal planes of (110) and (200) of a cubic FeCo alloy respectively (JCPDS No 44-1433). The unit cell parameter was calculated using the (110) reflection, giving a value of a 2.853 Å, which corresponds to the theoretical lattice constant reported in JCPDS No 44-1433 for disordered bcc-FeCo (2.857 Å) [47]. Therefore the synthesis method followed in our work does not lead to the equilibrium phase reported for the Fe/Co equiatomic composition at room temperature (the ordered α^t-ClCs phase) [21], but to a metastable disordered state. This is a consequence of the cooling process from the high temperatures reached during the CVD down to room temperature. The observation of metastable phases is in agreement with what is reported by authors following synthesis methods in which fast cooling rates are achieved [44, 12]. The absence of a diffraction peak at about 26.2° suggests that either the sample contains amorphous graphite [24] or, if the graphite is crystallized, the sample contains a small amount. No XRD reflections assignable to pure metal or to metal oxides were observed, indicating that the FeCo alloy is the only constituent of the magnetic nuclei. The average crystal size of the magnetic FeCo core was estimated to be 7.33 nm, using the Scherrer formula with consideration of K=0.8551 [23] and the FWHMs (full widths at half maximum) of the (110) peaks of the FeCo/CG diffractograms.

Figure 2(a) provides a representative TEM image of the FeCo/CG nanoparticles. Figure 2(b) corresponds to the particle size distribution fitted assuming a normal distribution. The particle size distribution was obtained by individual measurements of about 150 nanoparticles from different TEM images. Spherically shaped nanoparticles were obtained with a mean particle diameter of 6.85 1.27 nm, where, according to the upper panel of figure 2(b), 90% of the

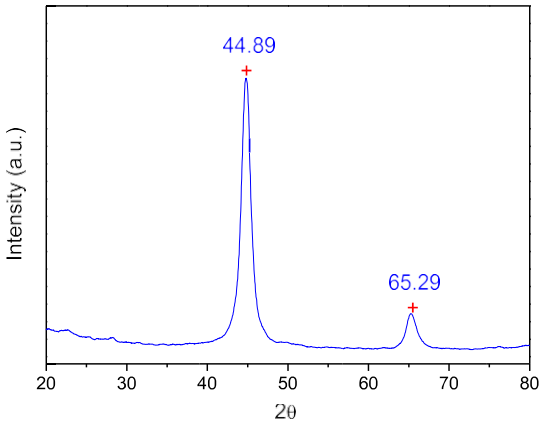

Figure 1. Powder XRD analysis diffractogram of the as-synthesized FeCo/CG nanoparticles.

FeCo/CG synthesized particles were under 8 nm diameter in good correspondence with the mean particle size from XRD results. This result is also in good agreement with the findings of Seo *et al* [46], who obtained a mean diameter of 7 nm using a weight $FeCo/SiO_2$ ratio of 0.041. Figure 2(c) shows a close-up view of the metallic nanoparticles where encapsulation by 3–5 graphitic carbon layers is clearly observed. This prevents particle nuclei agglomeration [5] and protects them from oxidation, as shown in the discussion below.

The aberration (C_s) corrected STEM was used to analyze the crystallographic structure of individual nanoparticles as well as their composition. Figure 3(a) displays a C_s corrected STEM-HAADF image of a highly crystalline bimetallic bcc nanoparticle, oriented along the [111] zone axis. The d-spacing of the {110} planes was measured to be 2.1 Å, giving a unit cell parameter value of 2.96 Å, very close to the theoretical value. The chemical composition of the produced nanoparticles was studied by STEM–EELS analysis. Figure 3(b) displays a spectrum acquired from the nanoparticle indicated by a white arrow (after background subtraction using the power law fit), showing the Fe $L_{2,3}$ and Co $L_{2,3}$ edges (at energy losses of 708 and 779 eV respectively). The absence of the O K edge at 532 eV confirms the protection from oxidation given by the carbon shell. A more general analysis is presented in figure 3(c) where chemical mappings extracted from STEM–EELS spectrum images were carried out, confirming the alloy formation through the simultaneous presence of Fe and Co in every particle analyzed, without any observable phase segregation. The EDS analysis (not shown) reported a Fe/Co ratio of1.08.

Surface analysis was performed by XPS spectroscopy to confirm the chemical species present in the nanoparticles. XPS spectra only showed the presence of C, Fe and Co, again corroborating the absence of oxides, and a Fe/Co atomic ratio of 0.99, in good agreement with EDS results. High-resolution spectra in the Fe 2p energy range (not shown) presented the Fe $2p_{3/2}$ peak at 707.5 eV and the Fe $2p_{1/2}$ one at 720.5 eV. The Co $2p_{3/2}$ is at 778.7 eV and the Co $2p_{1/2}$ is at 793.6 eV,

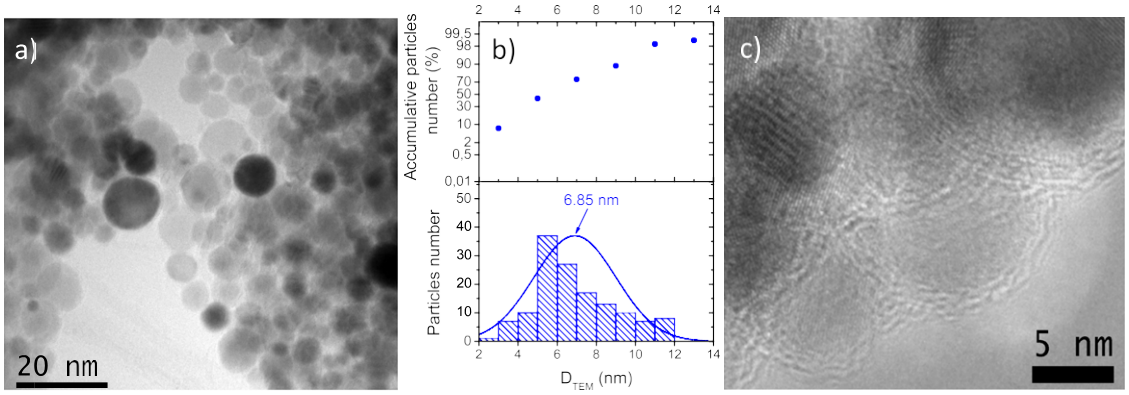

Figure 2. (a) TEM micrograph of the FeCo/CG nanoparticles. (b) Size distribution and (c) TEM image of the carbon layers.

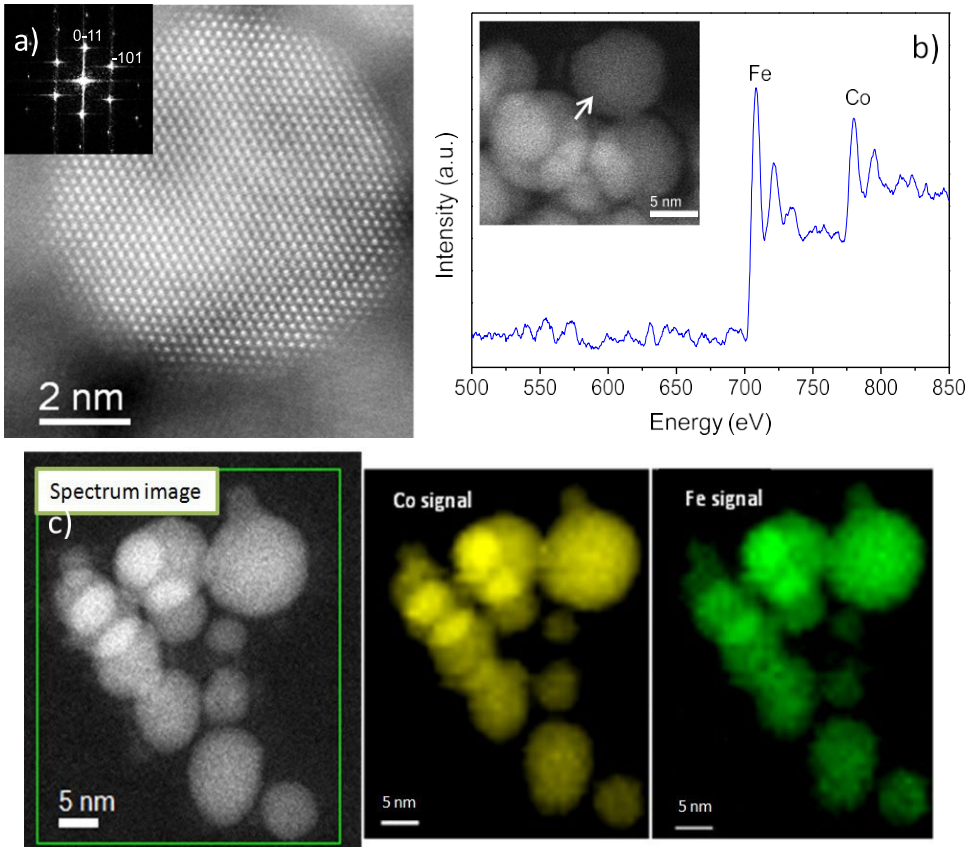

Figure 3. (a) Atomic resolution C_s corrected STEM-HAADF image of an as-synthesized FeCo/CG nanoparticle. (b) Point EELS spectrum of a FeCo/CG nanoparticle. (c) EELS chemical mapping from synthesized nanoparticles.

in good agreement with values previously reported for FeCo alloys [13]. There is no sign of Fe or Co oxidation—the presence of oxides would lead to the appearance of peaks at higher binding energies and with higher differences between the energy of the doublet components. Binding energies at 709.2 and 710.6 eV with BE $2p_{1/2}$ – BE $2p_{3/2}$ = 13.2 and 13.5 eV were reported for Fe^{2+} and Fe^{3+} respectively [27]. The Co $2p_{3/2}$ peak appears at 781.0 and 780.0 eV for Co^{2+} and Co^{3+} respectively [25].

Information concerning the carbon shell was obtained from the Raman spectroscopy; the results are shown in figure 4(a). For the as-synthesized nanoparticles three bands were observed in the spectra.

The band around 1330 cm^{-1} (D-band) is characteristic of the defects of carbon microtextures [58]. The most intense band at 1588 cm^{-1} (G-band), corresponds to the graphite-like band and is related to the vibration of sp^2-hybridized carbon atoms in the graphite layer [62]. The shoulder of this peak, observed at 1530–1540 cm^{-1}, would be related to the A-band, ascribed to amorphous carbon [58]. The predominance of the G-band suggests that well-defined graphite domains are developed, even though lattice defects in the graphite layers and some amorphous carbon are present.

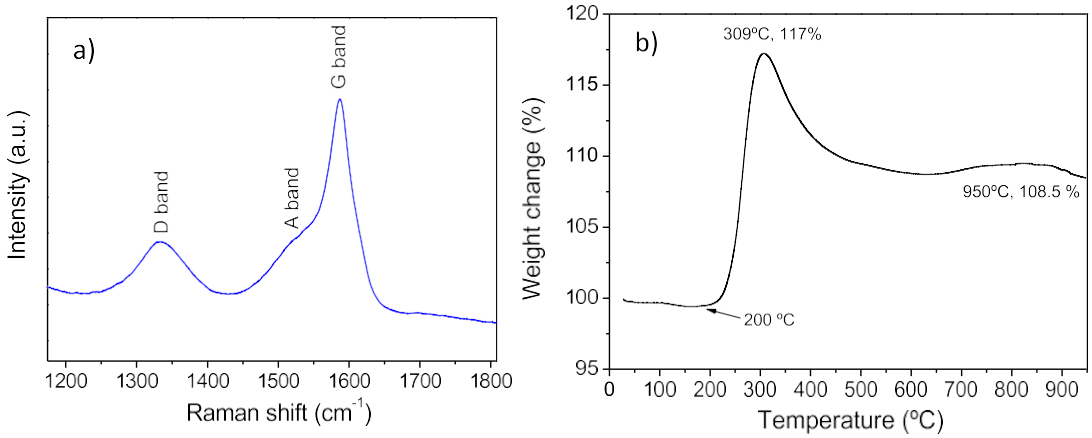

Figure 4. (a) Raman spectrum of FeCo/CG nanoparticles, (b) TGA curve of FeCo/CG nanoparticles under oxidizing atmosphere.

The influence of the graphitic layer on the thermal stability of the FeCo/CG nanoparticles was tested by thermogravimetric analysis. The samples were heated from 30 to 900 °C at 5 °C min^{-1} under O_2 atmosphere. Figure 4 shows the TGA profile, where a stable weight is observed until approximately 200 °C, followed by a steep weight gain, associated with the progressive oxidation of the nanoparticles due to the progressive disappearance of the graphitic coating [26]. A maximum is reached at 309 °C, when presumably the oxidation of the particle nuclei is nearly complete, and the weight loss due to the oxidation of carbon to CO_2 is the predominant process. The carbon content of the FeCo/CG nanoparticles was estimated as 23 wt%, a value calculated from the relative weights of the initial carbon-coated nanoparticles and of the final carbon-free oxidized particle nuclei. The oxidation state of the nanoparticles after the thermal treatment was determined by XPS analysis (not shown).

In order to investigate the magnetic properties of the synthesized nanoparticles, zero-field cooled (ZFC) and field cooled (FC) magnetization were measured under a magnetic field of 100 Oe in the temperature range from 10 K up to 350 K. Magnetization in emu per gram of FeCo (emu/g_{FeCo}) was calculated using the FeCo content obtained by TGA.

Figure 5 shows the zero-field cooled (ZFC) and field cooled (FC) magnetization curves up to 350 K. The ZFC magnetization curve shows a monotonic increase in the entire temperature range and does not merge with the FC curve. These facts suggest that the blocking temperature above which our nanoparticles would behave as a superparamagnetic system is higher than 350 K. Additionally, the FC magnetization curve remains almost constant in the measured temperature range, indicating the presence of strong dipolar magnetic interactions [37].

The magnetization of the as-synthesized FeCo/CG nanoparticles was measured as a function of the applied magnetic field up to 50 kOe at different temperatures, in the range between 10 and 300 K. The remnant field trapped in the superconducting magnet after the application of fields larger than 10 kOe has been characterized independently, by measuring a paramagnetic sample. It is −16 Oe, after the application of H = 50 kOe, and 16 Oe after the application of H = −50 kOe. The coercive fields reported have been corrected accordingly. The hysteresis loop at 300 K, shown in figure 6, suggests a superparamagnetic behavior for FeCo/CG nanoparticles at room temperature. However, a closer inspection at low fields (see inset figure 6) reveals that the magnetization curve displays a slight irreversibility, with small coercive field of 18.5 Oe indicating that the blocking temperature is above RT, in agreement with the ZFC/FC experiments. The coercive field of 18.5 Oe is in agreement with values reported for nanocomposite Fe–Co alloys (see discussion below), well known as soft magnetic materials, particularly around the equiatomic composition [53]. At the maximum applied field (50 kOe) the nanoparticles saturation magnetization reached 233 emu/g_{FeCo}, in the range of the saturation magnetization reported for FeCo nanoparticles at room temperature [7, 46, 60].

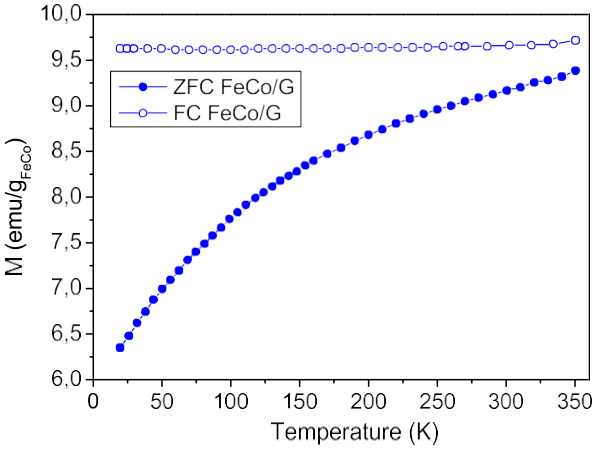

Figure 5. Temperature dependence of the ZFC/FC magnetization, under $H = 100$ Oe.

The saturation magnetization, M_s, was measured at 200, 100, 80, 50, 20 and 10 K. It is extrapolated to 0 K following the expression for nanoscale particles [16] $M_s(T) = M_{s(T=0K)}(1 - BT^{\alpha})$ (extrapolation not shown). The extrapolation at 5 K $M_{s(\ )} =$ 236.95 emu g^{-1} is in good agreement with the value reported at 5 K by Gallagher *et al*

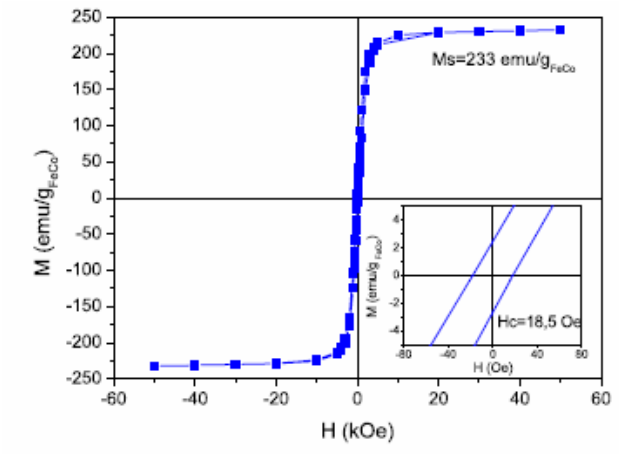

Figure 6. Magnetization isotherm at 300 K. Inset: low field magnetization.

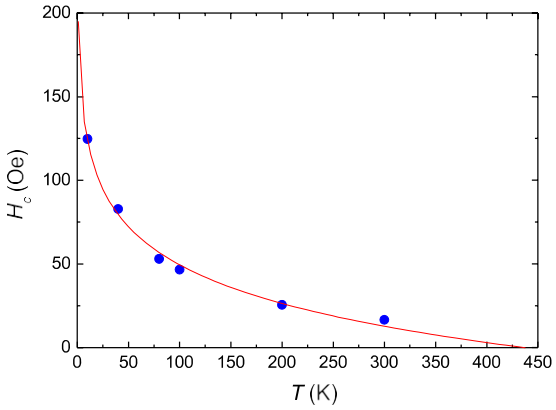

Figure 7. Dependence of the coercivity with temperature. The red line is a least-squares linear fit to equation (1).

for FeCo nanocrystals [12]. The extrapolation at 0 K yields $M_{s(T=0K)}$=236.98± 0.05 emu g^{-1}, which is a high value for a nanoparticle of average particle size of 7 nm. It is of the order of that reported by Bardos *et al* for the slow cooled bulk Fe–Co alloy (236.04 emu g^{-1}) [3]. Nevertheless, our nanoparticles have been fast cooled, and therefore, a value closer to that of fast quenched bulk alloy (according to Bardos $M_{s(T=0K)}$ ~ 229.16 emu g^{-1}) was expected instead. This inconsistency can be explained by a higher atomic diffusivity in nanometric systems as compared to the bulk, as already pointed out by Turgut *et al* [54], leading to some long range chemical order within the nanoparticle. In Fe–Co bulk alloys with Co contents between 5 and 70% the Co magnetic moment presents a value similar to that of an isolated Co atom (1.8 μ_B/Co atom), while the value of the Fe magnetic moment depends on the Co content [3]. The increase of Co nearest neighbors leads to an increase of the Fe magnetic moment and therefore to an increase of M_s. Under this assumption, the Fe magnetic moment of our nanoparticles is 3.06 μ_B, taking into account that the value of M average magnetic moment of 2.43 μ_B/atom. This value of the Fe magnetic moment indicates that the long range chemical order of the synthesized nanoparticles is close to the bulk, according to what is reported in [3].

In order to determine the magnetocrystalline anisotropy constant the coercivity temperature dependence was also studied. The coercive field (H_c) values as a function of the temperature are presented in figure 7, showing a monotonic increase as the temperature decreases.

The dependence of H_c on nanoparticle size and temperature was first described by Kneller and Luborsky for non-interacting nanoparticles, with uniaxial anisotropy [22]. The energy barrier for the reversal of the magnetization was expressed as $E = K_{eff} \times V(1 - \frac{HM_s}{2K_{eff}})^2$, where K_{eff} is the anisotropy constant. The energy barrier must be sufficiently reduced by the applied magnetic field H, so that the magnetization reversal occurs during the measurement time. Considering as usual for dc measurements $E = 25k_BT$ the coercive field is such that verifies $25k_BT = K_{eff}\ V(1-HcMs/2Keff)^2$. Then Hc(T)=($2Keff$ /Ms)(1-T/T$_B$)$^{1/2}$, where T$_B$ =$Keff$ V/25k$_B$.

is the temperature below which the magnetic moment of the particle with anisotropy energy $K_{eff}V$ becomes blocked. The former expression for $H_c(T)$ can be generalized by substituting the exponent (1/2) by α [39]. Simulations and experimental results show that α mainly depends on the interparticle interactions [34, 39] but also on the particle morphology and size distribution. Concerning interactions, at temperatures much lower than T_B, both magnetization and coercivity decrease with temperature more steeply compared to the non-interacting case. Approaching T_B, M_r and H_c have much slower decay with temperature, conserving the blocked character up to temperatures above the non-interacting T_B. These features are in agreement with our results shown in figure 7. Assuming that particle easy axes are randomly oriented, the expression of the coercive field becomes

$$H_c(T) = 0.48 \times \frac{2K_{eff}}{M_s} \times \left(1 - \left(\frac{T}{T_B}\right)^{\alpha}\right)$$

The fit of the temperature dependence of the coercive field to this expression (figure 7) gives the anisotropy constant K_{eff}= 4.17x10^5 erg g^{-1}, in agreement with reported values for FeCo nanocomposites [20]. Notice that, as already pointed out by Ibrahim *et al*, it is two orders of magnitude larger as compared to the bulk value K_{eff} ~ 10^4 erg cm^{-3} [38]. Such an enhancement of the anisotropy can be attributed to surface effects [20], distorted lattices and/or reduced symmetry in FeCo nanoparticles [1, 2, 4]. Additionally, a large magnetic anisotropy constant is expected in fast cooled disordered FeCo alloys, as our system, compared with that of slowly cooled ordered ones [14]. The α exponent = 0.02 obtained in the present fit is in agreement with that reported for 10 nm γ -Fe$_2$O$_3$ nanoparticles [42, 48]. The blocking temperature determined from the fit is T_B =437.1 ± 35.5 K, which is larger than the one that can be estimated for non-interacting magnetic nanoparticles. The relaxation time for a system with non-interacting nanoparticles follows $\tau = \tau_0 e^{\frac{KV}{k_B T}}$ which for the experimental time τ used in the magnetization experiments gives 25= KV/k$_B$T$_B$.
Then, for a particle with a diameter of 6.85 nm using the value of K_{eff} derived from the fitting the calculated blocking temperature

is $T_B \approx 176$ K, much smaller than the blocking temperature obtained from the fit to the $H_c(T)$ model for interacting nanoparticles. This fact shows that though the synthesized nanoparticles are not aggregated the interactions between their magnetic moments are significant, in agreement with the FC experiments discussed previously.

In order to investigate the magnetic properties of the FeCo nanoparticles in the working temperature range of their future application in magneto-responsive composites, the magnetization was measured heating at 10 K min^{-1} the synthesized powders from room temperature up to 477 °C (750 K), applying 100 Oe. The measurements were performed using the MPMS oven option, in a specially designed quartz sealed sample holder. The diamagnetic signal arising from the sample holder was negligible in comparison with the sample signal. The results are presented in figure 8. The magnetization continuously increases from 300 K (see figure 8(a)), in agreement with that observed in the ZFC magnetization curve. A broad maximum is observed centered at 400 K that could be tentatively ascribed to the progressive change from the blocked state of the nanoparticles at room temperature to a superparamagnetic one. At 367 °C (640 K) an anomalous increase of the magnetization with the temperature takes place. This feature was also observed in carbon-coated FeCo nanocrystals [44, 53]. It was assigned to a gradual ordering upon heating the metastable disordered bcc phase in which the as-synthesised nanoparticles crystallize towards the transition to the ordered bcc α^t-ClCs-type phase. This order–disorder transition within the bcc phase was previously observed in the bulk FeCo alloy, taking place approximately at 457 °C (730 K) [54]. Such atomic reordering would also homogenize the distribution of the Fe and Co atoms in the particle, increasing the number of neighboring Co surrounding a Fe atom. Since the magnetic moment of the iron atom increases with the number of Co neighbors [3], the total magnetization would increase, correspondingly. After this thermal treatment, once the applied magnetic field was switched off, the sample was cooled down at sweeping rate slower than 10 K min^{-1} to room temperature, and a new magnetization measurement on heating was registered (figure 8(a)). The maximum is now broader, appearing centered at about 500 K and the initial state in the second annealing process is different from that corresponding to the first thermal treatment. The fact that the magnetization in the whole temperature range does not reproduce the behavior observed during the preceding thermal treatment agrees with the results reported by Turgut *et al* [53] and Scott *et al* [44] which in turn resemble previous observations in bulk Fe–Co–V alloys. Evidence of magnetization changes after heat treatments up to 477 °C (750 K) is also displayed in the hysteresis curve shown in figure 8(b), measured at 300 K after the thermal treatment (unfilled symbols). The hysteresis loop measured before the treatment is also included for comparison. Notice that after the treatment the saturation magnetization increased to 257 emu/g_{FeCo}, supporting the atomic reordering in the nanoparticle previously discussed. The coercive field increases as well from 18.5 Oe before heating up to 25.5 Oe after the thermal treatment. Though

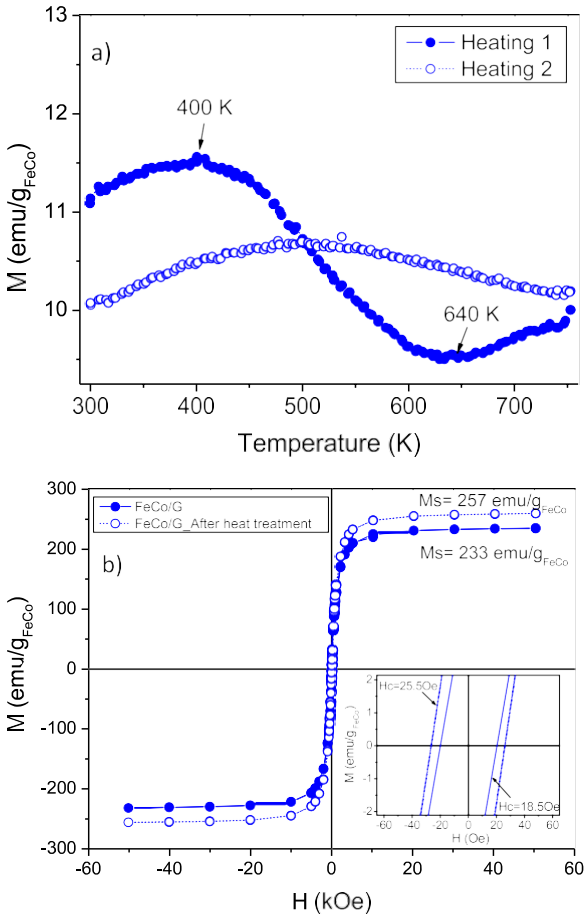

Figure 8. Magnetic characterization of FeCo/CG. (a) Heating curves in the high temperature range under H= 100 Oe, (b) comparison of magnetization isotherms at 300 K, before and after high temperature heat treatments. Inset: low field magnetization.

the difference seems not very large, this feature is in fact remarkable. First, it is in disagreement with the coercive field decrease after heating treatments reported previously (e.g. by Turgut *et al* [53]). Moreover, after this thermal processing the sample was cooled down by thermal radiation to 300 K. This is even slower than the cooling process followed after the CVD synthesis, and therefore an ordering to a more stable structure can be expected. In slowly cooled FeCo alloys the magnetic anisotropy constant is smaller as compared to that of fast quenched ones [14]. Also, saturation magnetization increased and therefore $H_c = 2$ K/M_s is expected to be smaller after the thermal processing. This inconsistency concerning the variation of H_c after annealing will be discussed below.

In order to study the origin of the observed changes in the magnetic behavior, two additional tests were carried out: a thermomagnetic analysis (TMA), and a differential scanning calorimetry (DSC). The TMA curve recorded at 5 °C min^{-1} (figure 9) shows an apparent weight increase from 36 to 150 °C (309–423 K) and then a decrease from 150 to 400 °C (423–673 K). These changes in the magnetization are in good agreement with those observed during the first thermal treatment (figure 8(a)).

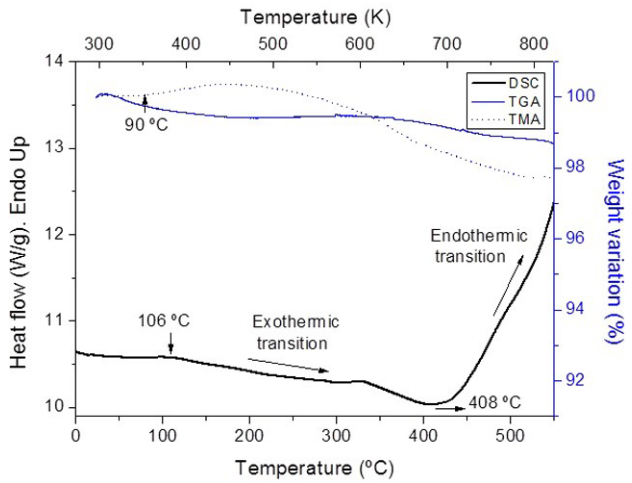

Figure 9. TGA, TMA and DSC thermograms of FeCo/CG nanoparticles, under continuous N_2 flow.

The DSC results are presented in figure 9. An exothermic process takes place from 100 to 425 °C. From 425 °C up to 550 °C, an endothermic process occurs. In agreement with [44, 53, 54], an atomic ordering of the as-synthesized quenched disordered bcc phase takes place when heating from room temperature up to at least 500 °C. Scott *et al* observed the appearance in this temperature range of the superlattice (100) peak in the neutron diffraction experiments reported in [44]. This atomic ordering corresponds to an exothermic process [41, 51], and takes place in the same temperature range at which the magnetization measured in the first thermal treating starts to increase, as shown in figure 8. As discussed before, these temperature induced changes in the magnetization evidence changes in the Fe atomic neighborhood, and have been also reported by Turgut *et al* in [53, 54].

On the other hand, changes in the graphite structure are expected in the temperature range of our DSC measurements. According to the results on graphite films grown by PLD reported by Friedman *et al* [11], the thermal stability of the obtained specimens is highly dependent on the synthesis atmosphere. These authors found that N_2 and H_2 were incorporated into the film structure and that the thermal stability of films grown in N_2 or H_2 atmosphere was very low when annealing up to 800 °C (1073 K). They conclude that the N_2 is eliminated when warming up to approximately 400 °C (673 K), leading to an increase of the amorphous carbon fraction present in their samples. The study carried out by Misra *et al* [32] on nitrogen doped carbon nanotubes grown by microwave plasma chemical vapor deposition (MPCVD) concludes that nitrogen and hydrogen are chemisorbed as impurities in the carbon structure leading to defects and to N–CH_3, C–N and C–H bonds. FTIR and TGA/DTA studies showed that a gradual removal of the nitrogen and hydrogen bonded species takes place between 400 °C (673 K) and 600 °C (873 K), simultaneously to the evaporation of amorphous carbon and to the annealing of the defects induced by the presence of nitrogen.

The presence of defects and amorphous carbon co-existing with crystallized graphite has been evidenced in the Raman spectra of our as-synthesized nanoparticles (figure 4(a)). Therefore, in the temperature interval of our DSC measurements the exothermic process associated with the gradual ordering of the metastable disordered bcc phase is superimposed on the endothermic one ascribed to the changes in the graphite coating. Up to 425 °C (698 K) the exothermic changes taking place in the FeCo alloy dominate and from this temperature up to 550 °C (823 K) the endothermic processes are predominant. As in [32] a sample weight loss has been observed in our TGA results, associated with the removal of N/H species and of amorphous carbon. No endothermic processes associated with changes in the FeCo alloy are expected in the measured temperature range because, as has been already reported [9, 31, 44, 54], no transitions are expected up to about 927 °C (approximately 1200 K), at which temperature the transition from ordered bcc structure to the fcc phase takes place.

To study any possible changes in the morphology and chemical composition of the nanoparticles that could take place together with the observed changes in the magnetization, coercive field and anisotropy mentioned in the previous paragraphs, as well as with the transitions observed in the thermal analysis, a characterization of the nanoparticles after heating up to 477 °C (750 K) was performed by means of HRSTEM techniques. Figure 10 displays the STEM micrographs of nanoparticles. From the low magnification image (figure 10(a)) it can be seen that nanoparticles still remain largely as individual entities and that their mean diameter does not present any significant change, (being around 6.03 $\pm$0.82 nm), ruling agglomeration out as a consequence of heating. In addition, a closer observation of the material shows that nanoparticles have evolved into faceted crystals. Figure 10(b) displays two typical C_s corrected STEM-HAADF images of the nanoparticles after heating which clearly show the faceting of the surface. The bottom part of figure 10(b) depicts a truncated cube oriented on its [100] zone axis. The interatomic distances, measured in both particles, correspond to a bcc structure with a $d_{(110)} = 0.194$ nm giving a unit cell value of $a = 2.73$ Å, in agreement with the corresponding values of the as-synthesized material (see figure 2(b)). The observed faceting is theoretically predicted for crystal sizes lower than 1.5–2 nm [29] but also occurs as a consequence of energy surface minimization leading to a more energetically favorable structure [29, 36]. In the present case the annealing temperature is not enough to induce the complete ordering of the Fe and Co atoms to stabilize the equilibrium ordered σ^t-ClCs phase, and therefore truncation takes place in order to reach the thermodynamic equilibrium.

Such a situation has been observed in nanoparticles after an oxidation process [6]. However, in our case the graphite coating still remained after the thermal treatments, preventing oxidation of the FeCo nuclei. The coating is clearly seen in figure 10(c). Moreover, the absence of oxidation has been confirmed by the magnetization measurements shown in figure 8(b) and by EELS and XPS analyses (not shown).

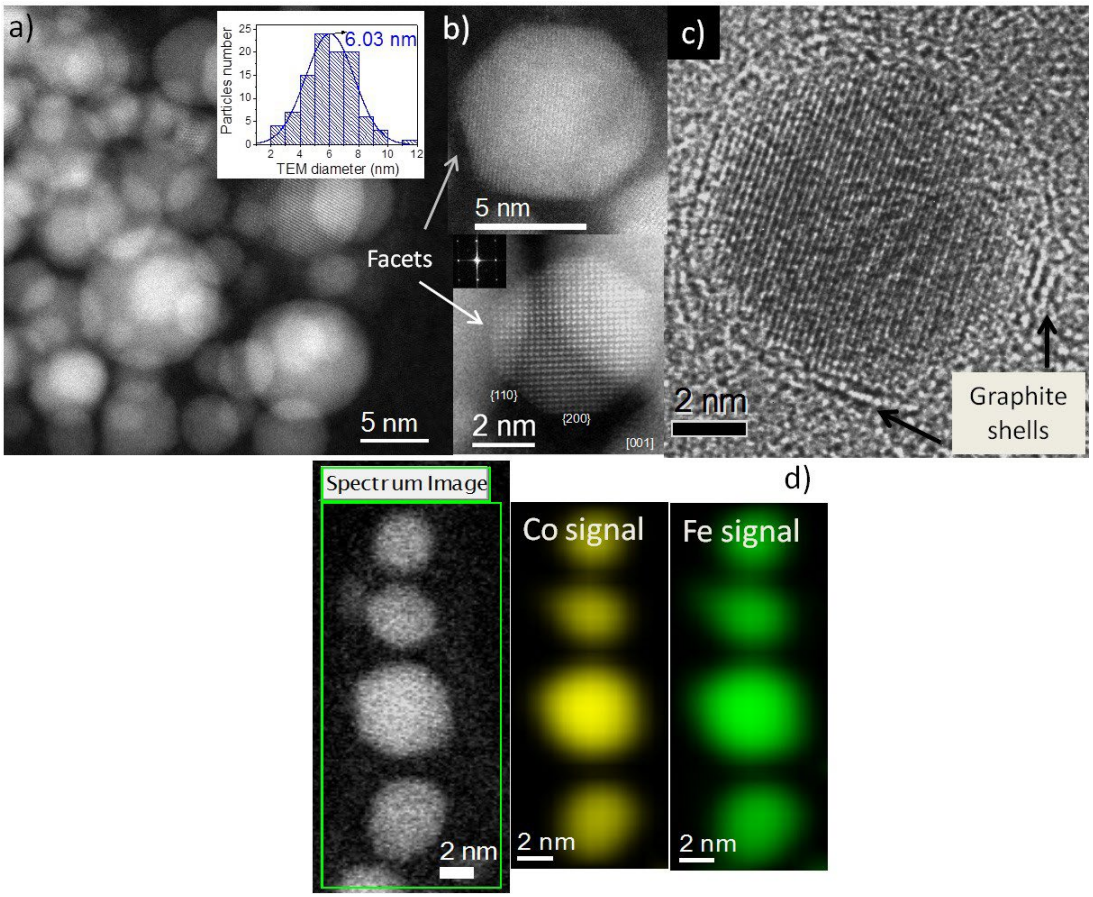

Figure 10. Aberration corrected STEM images of the FeCo/CG after heating up to high temperature. (a) Low magnification HAADF micrograph. Inset: size distribution histogram. (b) Atomic resolution image and (c) BF image showing several graphitic layers. (d) EELS chemical mapping.

In our case, the faceting is favored by the temperature induced changes in the graphite coating taking place during the particle heating, as explained in the analysis of the DSC results. As far as we know, such faceting taking place simultaneously with the ordering within the bcc metastable phase has not been shown previously. This faceting of the nanoparticle surface is crucial to understand the inconsistency reported previously with respect to the increase of the coercive field after the thermal treatment. The increase of H_c cannot be explained in terms of the variation of the magnetocrystalline constant but can be explained in terms of a shape anisotropy that becomes dominant after the annealing process. Magnetocrystalline anisotropy in FeCo alloy decreases after the thermal treatment, as reported for slowly cooled bulk FeCo alloys [14], in agreement with results reported in previous papers (e.g. by Turgut *et al* [53]). Also, since after the thermal treatment the sample was slowly cooled by thermal radiation, an atomic ordering to a more stable structure is expected, leading to larger saturation magnetization and to a lower value of the magnetocrystalline anisotropy constant. However, faceting induces a shape anisotropy in the particle that overrides magnetocrystalline anisotropy leading to a higher H_c after annealing.

As an example, the chemical map of four nanoparticles is shown in figure 10(d). The compositional analysis corroborates that the Fe and Co are homogeneously distributed in all the crystals. This again indicates that the magnetization increment is not related to any composition change and even less to a FeCo oxidation (which would lead to a decrease of the magnetization).

4. Conclusions

In summary, alloyed $Fe_{50}Co_{50}$ nanoparticles protected by a graphite phase have been produced by a high temperature reduction method. The nanoparticles originally presented a spherical morphology with mean diameter of 6.85 $\pm$.27 nm and a homogeneous composition of both elements. It was found that the carbon shell preserved the nanoparticles stable under oxidizing atmosphere, preventing particles sintering and oxide formation. In addition, XRD analysis and atomic resolution electron microscopy revealed a very good crystallinity in the metastable disordered bcc-FeCo phase with long range chemical order close to the bulk; meanwhile, magnetization analysis exhibited large magnetization parameters in the ferromagnetic regime.

The existence of structural and magnetic temperature induced transitions changes from 36 °C (309 K) up to 477 °C (750 K), leading to an increase in magnetization from

233 up to 257 emu/g_{FeCo} and H_c from 18.5 to 25.5 Oe, was assessed. In this aspect, no diameter variations or compositional changes of the nanoparticles were observed; however, a higher faceting appeared as a consequence of the atomic reorganization to reach the thermodynamic equilibrium within the metastable phase. Such results confirm that the magnetic, chemical and physical properties of synthesized FeCo/CG nanoparticles will not be negatively affected in the working temperature range of their future application in magneto-responsive composites; instead higher magnetization and stable ordered bcc-FeCo phase is obtained.

Acknowledgments

AU acknowledges financial support from DGA-E8-MOLCHIP and MAT2012-38318-C03-03 projects. The authors would like to acknowledge the use of Servicio General de Apoyo a la Investigación-SAI, Universidad de Zaragoza.

References

[1] Andersson G, Burkert T, Warnicke P, Björck M, Sanyal B, Chacon C, Zlotea C, Nordström L, Nordblad P and Eriksson O 2006 Perpendicular magnetocrystalline anisotropy in tetragonally distorted Fe–Co alloys Phys. Rev. Lett. **96** 037205

[2] Bansmann J, Kleibert A, Getzlaff M, Rodr´ıguez A F, Nolting F, Boeglin C and Meiwes-Broer K-H 2010 Magnetism of 3d transition metal nanoparticles on surfaces probed with synchrotron radiation—from ensembles towards individual objects Phys. Status Solidi b **247** 1152–60

[3] Bardos D I 1969 Mean magnetic moments in bcc Fe–Co alloys J. Appl. Phys. **40** 1371

[4] Burkert T, Nordström L, Eriksson O and Heinonen O 2004 Giant magnetic anisotropy in tetragonal FeCo alloys Phys. Rev. Lett. **93** 027203

[5] Castrillon M, Mayoral A, Magen C, Meier J G, Marquina C, Irusta S and Santamaria J 2012 Synthesis and characterization of ultra-small magnetic FeNi/G and NiCo/G nanoparticles Nanotechnology **23** 085601

[6] Collier K N, Jones N J, Miller K J, Qin Y L, Laughlin D E and McHenry M E 2009 Controlled oxidation of FeCo magnetic nanoparticles to produce faceted FeCo/ferrite nanocomposites for RF heating applications J. Appl. Phys. **105** 07A328

[7] Chaubey G S, Barcena C, Poudyal N, Rong C, Gao J, Sun S and Liu J P 2007 Synthesis and stabilization of FeCo nanoparticles J. Am. Chem. Soc. **129** 7214

[8] Chen Z, Hong G, Wang H, Welsher K, Tabakman S M, Sherlock S P, Robinson J T, Liang Y and Dai H 2012 Graphite-coated magnetic nanoparticle microarray for few-cells enrichment and detection ACS Nano **6** 1094–101

[9] Davis J 2007 Nickel, Cobalt and their Alloys (Ohio: ASM International)

[10] Desvaux C, Lecante P, Respaud M and Chaudret B 2010 Structural and magnetic study of the annealing of Fe–Co nanoparticles J. Mater. Chem. **20** 103–9

[11] Friedmann T A, McCarty K F, Barbour J C, Siegal M P and Dibble D C 1996 Thermal stability of amorphous carbon films grown by pulsed laser deposition Appl. Phys. Lett. **68** 1643–5

[12] Gallagher K, Johnson F, Kirkpatrick E M, Scott J H, Majetich S and McHenry M E 1996 Synthesis, structure, and magnetic properties of Fe–Co alloy nanocrystals IEEE Trans. Magn. **32** 4842–4

[13] Gao X Y, Tan S C, Wee A T S, Wu J, Kong L B, Yu X J and Moser H O 2006 Structural and magnetic characterization of soft-magnetic FeCo alloy nanoparticles J. Electron Spectrosc. Relat. Phenom. **150** 11–4

[14] Hall R C 1960 Magnetic anisotropy and magnetostriction of ordered and disordered cobalt–iron alloys J. Appl. Phys. **31** S157–8

[15] Harris P J F and Tsang S C 1998 A simple technique for the synthesis of filled carbon nanoparticles Chem. Phys. Lett. **293** 53–8

[16] Hendriksen P V, Linderoth S and Lindgård P A 1993 Finite-size modifications of the magnetic properties of clusters Phys. Rev. B **48** 7259–73

[17] Hisada D, Fujiwara Y, Sato H, Jimbo M, Kobayashi T and Hata K 2011 Structure and magnetic properties of FeCo nanoparticles encapsulated in carbon nanotubes grown by microwave plasma enhanced chemical vapor deposition J. Magn. Magn. Mater. **323** 3184–8

[18] Holodelshikov E, Perelshtein I and Gedanken A 2011 Synthesis of air stable FeCo/C alloy nanoparticles by decomposing a mixture of the corresponding metal–acetyl acetonates under their autogenic pressure Inorg. Chem. **50** 1288–94

[19] Huba Z J, Carroll K J and Carpenter E E 2011 Synthesis of high magnetization FeCo alloys prepared by a modified polyol process J. Appl. Phys. **109** 07B514

[20] Ibrahim E M M et al 2012 Superparamagnetic FeCo and FeNi nanocomposites dispersed in submicrometer-sized C spheres J. Phys. Chem. C **116** 22509–17

[21] Jeyadevan B, Shinoda K, Justin R J, Matsumot T, Sato K, Takahashi H, Sato Y and Tohji K 2006 Polyol process for Fe-based hard(fct-FePt) and soft(FeCo) magnetic nanoparticles IEEE Trans. Magn. **42** 3030–5

[22] Kneller E F and Luborsky F E 1963 Particle size dependence of coercivity and remanence of single-domain particles J. Appl. Phys. **34** 656

[23] Langford J I and Wilson A J C 1978 Scherrer after 60 years—survey and some new results in determination of crystallite size J. Appl. Crystallogr. **11** 102–13

[24] Lee S J, Cho J-H, Lee C, Cho J, Kim Y-R and Park J K 2011 Synthesis of highly magnetic graphite-encapsulated FeCo nanoparticles using a hydrothermal process Nanotechnology **22** 375603

[25] Lin S S Y, Kim D H, Engelhard M H and Ha S Y 2010 Water-induced formation of cobalt oxides over supported cobalt/ceria–zirconia catalysts under ethanol-steam conditions J. Catal. **273** 229–35

[26] Liu X G, Ou Z Q, Geng D Y, Han Z, Jiang J J, Liu W and Zhang Z D 2010 Influence of a graphite shell on the thermal and electromagnetic characteristics of FeNi nanoparticles Carbon **48** 891–7

[27] Martinez G, Malumbres A, Mallada R, Hueso J L, Irusta S, Bomati-Miguel O and Santamaria J 2012 Use of a polyol liquid collection medium to obtain ultrasmall magnetic nanoparticles by laser pyrolysis Nanotechnology **23** 425605

[28] Maryško M, Fajgar R, Šubrt J, Murafa N and Knížek K 2010 Magnetic properties of FeCo nanoparticles encapsulated in carbon J. Phys.: Conf. Ser. **200** 072065

[29] Mayoral A, Barron H, Estrada-Salas R, Vazquez-Duran A and Jose-Yacaman M 2010 Nanoparticle stability from the nano to the meso interval Nanoscale **2** 335–42

[30] McHenry M E, Willard M A and Laughlin D E 1999 Amorphous and nanocrystalline materials for applications as soft magnets Prog. Mater. Sci. **44** 291–433

[31] Meng L J, Peng X Y, Zhang K W, Tang C and Zhong J X 2012 Structural phase transitions of FeCo and FeNi nanoparticles: a molecular dynamics study J. Appl. Phys. **111** 024303

[32] Misra A, Tyagi P K, Singh M K and Misra D S 2006 FTIR studies of nitrogen doped carbon nanotubes Diamond Relat. Mater. **15** 385–8

[33] Mohr R, Kratz K, Weigel T, Lucka-Gabor M, Moneke M and Lendlein A 2006 Initiation of shape-memory effect by inductive heating of magnetic nanoparticles in thermoplastic polymers Proc. Natl Acad. Sci. USA **103** 3540–5
[34] Nunes W C, Novak M A, Knobel M and Hernando A 2001 Magnetic properties in granular $Co_{10}Cu_{90}$ alloys: the effect of random anisotropy and interparticle interactions J. Magn. Magn. Mater. **226–230** 1856–8
[35] Paraskevas L, Caps V and Tsang S C 2006 Syntheses of carbon encapsulated magnetic FeNi nanoparticle via decompositions of methane and benzene Carbon **44** 820–3
[36] Penuelas J, Andreazza-Vignolle C, Andreazza P, Ouerghi A and Bouet N 2008 Temperature effect on the ordering and morphology of CoPt nanoparticles Surf. Sci. **602** 545–51
[37] Pérez Alcázar G A, Zamora L E, Tabares J A, Piamba J F, González J M, Greneche J M, Martinez A, Romero J J and Marco J F 2013 Evidence of magnetic dipolar interaction in micrometric powders of the $Fe_{50}Mn_{10}Al_{40}$ system: melted alloys J. Magn. Magn. Mater. **327** 137–45
[38] Pfeifer F and Radeloff C 1980 Soft magnetic Ni–Fe and Co–Fe alloys—some physical and metallurgical aspects J. Magn. Magn. Mater. **19** 190–207
[39] Pfeiffer H 1990 Determination of anisotropy field distribution in particle assemblies taking into account thermal fluctuations Phys. Status Solidi a **118** 295–306
[40] Pol S V, Pol V G, Frydman A, Churilov G N and Gedanken A 2005 Fabrication and magnetic properties of Ni nanospheres encapsulated in a fullerene-like carbon J. Phys. Chem. B **109** 9495–8
[41] Porter D and Easterling K 1992 Phase Transformations in Metals and Alloys (London: Stanley Thornes)
[42] Read D A, Moyo T and Hallam G C 1984 Low-temperature magnetic hardness of melt spun Fe–Zr amorphous alloys J. Magn. Magn. Mater. **44** 279–86
[43] Robinson I, Zacchini S, Tung L D, Maenosono S and Thanh N T K 2009 Synthesis and characterization of magnetic nanoalloys from bimetallic carbonyl clusters Chem. Mater. **21** 3021–6
[44] Scott J H J, Chowdary K, Turgut Z, Majetich S A and McHenry M E 1999 Neutron powder diffraction of carbon-coated FeCo alloy nanoparticles J. Appl. Phys. **85** 4409–11
[45] Schmidt A M 2006 Electromagnetic activation of shape memory polymer networks containing magnetic nanoparticles Macromol. Rapid Commun. **27** 1168–72
[46] Seo W S et al 2006 FeCo/graphitic-shell nanocrystals as advanced magnetic-resonance-imaging and near-infrared agents Nature Mater. **5** 971–6
[47] Sourmail T 2005 Near equiatomic FeCo alloys: constitution, mechanical and magnetic properties Prog. Mater. Sci. **50** 816–80
[48] Sreeja V and Joy P A 2007 Microwave-hydrothermal synthesis of γ -Fe_2O_3 nanoparticles and their magnetic properties Mater. Res. Bull. **42** 1570–6
[49] Su X B, Zheng H G, Yang Z P, Zhu Y C and Pan A L 2003 Preparation of nanosized particles of FeNi and FeCo alloy in solution J. Mater. Sci. **38** 4581–5
[50] Thevenot J, Oliveira H, Sandre O and Lecommandoux S 2013 Magnetic responsive polymer composite materials Chem. Soc. Rev. **42** 7099–116
[51] Mettler Toledo GmbH 2000 Interpreting DSC Curves Part 1: Dynamic Measurements (Switzerland: UserCOM 11)
[52] Tomita S, Hikita M, Fujii M, Hayashi S and Yamamoto K 2000 A new and simple method for thin graphitic coating of magnetic-metal nanoparticles Chem. Phys. Lett. **316** 361–4
[53] Turgut Z, Huang M Q, Gallagher K, McHenry M E and Majetich S A 1997 Magnetic evidence for structural-phase transformations in Fe–Co alloy nanocrystals produced by a carbon arc J. Appl. Phys. **81** 4039–41
[54] Turgut Z, Scott J H, Huang M Q, Majetich S A and McHenry M E 1998 Magnetic properties and ordering in C-coated Fe_xCo_{1-x} alloy nanocrystals J. Appl. Phys. **83** 6468–70
[55] Tzitzios V, Basina G, Niarchos D, Li W and Hadjipanayis G 2011 Synthesis of air stable FeCo nanoparticles J. Appl. Phys. **109** 07A313
[56] Wang Z H, Choi C J, Kim B K, Kim J C and Zhang Z D 2003 Characterization and magnetic properties of carbon-coated cobalt nanocapsules synthesized by the chemical vapor-condensation process Carbon **41** 1751–8
[57] Wu W Z, Zhu Z P and Liu Z Y 2003 A study of the explosion of Fe–C hybrid xerogels and the solid products Carbon **41** 309–15
[58] Xue P, Gao J, Bao Y, Wang J, Li Q and Wu C 2011 An analysis of microstructural variations in carbon black modified by oxidation or ultrasound Carbon **49** 3346–55
[59] Yamada M, Okumura S-J and Takahashi K 2010 Synthesis and film formation of magnetic FeCo nanoparticles with graphitic carbon shells J. Phys. Chem. Lett. **1** 2042–5
[60] Zamanpour M 2012 Fabrication of Novel Magnetic Nanostructures Towards Efficient Powder Generation (Boston: Northeastern University, Department of Chemical Engineering)
[61] Zamanpour M, Chen Y, Hu B, Carroll K, Huba Z J, Carpenter E E, Lewis L H and Harris V G 2012 Large-scale synthesis of high moment FeCo nanoparticles using modified polyol synthesis J. Appl. Phys. **111** 07B528
[62] Zhu W, Ren J, Gu X, Azmat M U, Lu G and Wang Y 2011 Synthesis of hermetically-sealed graphite-encapsulated metallic cobalt (alloy) core/shell nanostructures Carbon **49** 1462–72
[63] Zin V and Dabala M 2011 Temperature dependent properties and aggregation behaviour of FeCo nanoparticles produced sonoelectrochemically J. Nanopart. Res. **13** 7253–62